Monovalent Ion Selectivity Sequences of the Rat Connexin43 Gap Junction Channel

Hong-Zhan Wang and Richard D. Veenstra

From the Department of Pharmacology, SUNY Health Science Center at Syracuse, Syracuse, New York 13210

ABSTRACT The relative permeability sequences of the rat connexin 43 (rCx43) gap junction channel to seven cations and chloride were examined by double whole cell patch clamp recording of single gap junction channel currents in rCx43 transfected neuroblastoma 2A (N2A) cell pairs. The measured maximal single channel slope conductances (γ_j, in pS) of the junctional current-voltage relationships in 115 mM XCl were RbCl (103) ≥ CsCl (102) > KCl (97) > NaCl (79) ≥ LiCl (78) > TMACl (65) > TEACl (53) and for 115 mM KY were KBr (105) > KCl (97) > Kacetate (77) > Kglutamate (61). The single channel conductance-aqueous mobility relationships for the test cations and anions were linear. However, the predicted minimum anionic and cationic conductances of these plots did not accurately predict the rCx43 channel conductance in 115 mM KCl. Instead, the conductance of the rCx43 channel in 115 mM KCl was accurately predicted from cationic and anionic conductance-mobility plots by applying a mobility scaling factor D_x/D_o, which depends upon the relative radii of the permeant ions to an estimated pore radius. Relative permeabilities were determined for all of the monovalent cations and anions tested from asymmetric salt reversal potential measurements and the Goldman-Hodgkin-Katz voltage equation. These experiments estimate the relative chloride to potassium permeability to be 0.13. The relationship between the relative cation permeability and hydrated radius was modeled using the hydrodynamic equation assuming a pore radius of 6.3 ± 0.4 Å. Our data quantitatively demonstrate that the rCx43 gap junction channel is permeable to monovalent atomic and organic cations and anions and the relative permeability sequences are consistent with an Eisenman sequence II or I, respectively. These predictions about the rCx43 channel pore provide a useful basis for future investigations into the structural determinants of the conductance and permeability properties of the connexin channel pore.

KEY WORDS: permeability • conductance ratio • hydrodynamic equation • Eisenman series • raffinose

INTRODUCTION

Gap junction channels, which are composed of two juxtaposed hexameric hemichannels, form intercellular pathways for the diffusion of ions and small molecules. Each hemichannel is formed by six protein (connexin) subunits that share major topological structure identity. In myocardium, electrical coupling through gap junctions facilitates action potential propagation through the specialized conducting tissues and organizes the working myocardium into a functional syncytium (Beyer et al., 1990; Brink, 1991; Veenstra, 1991). Functional expression of cloned connexin DNAs in *Xenopus* oocytes and communication-deficient mammalian cell lines exhibit distinct transjunctional voltage sensitivities and unitary channel conductances (Swenson et al., 1989; Werner et al., 1989; Fishman et al., 1990, 1991; Veenstra et al., 1992; Reed et al., 1993; Rup et al., 1993). Distinct ionic and dye permeabilities of chick connexin45 and human connexin37 gap junction channels have been reported (Veenstra et al., 1994*a*, *b*). In contrast, rat connexin43 (rCx43, one of the major connexins in rat and all other mammalian heart) gap junction channels transfected into the same neuroblastoma 2A (N2A)[1] cells exhibit only a weak relative anion:cation selectivity ratio (≈1) and are readily permeable to the anionic fluorescein dye derivatives 6-carboxyfluorescein and 2,7-dichlorofluorescein (Veenstra et al., 1995). The molecular basis for this weak ionic and molecular selectivity remains unknown, but the results are consistent with a weak anionic field associated with a site within a >10 Å diameter pore of the rCx43 channel. The relative strength of electrostatic field potentials have been ascertained for other ion selective channels by determining the characteristic monovalent cation selectivity sequence (Eisenman series I-XI, Eisenman and Horn, 1983). Furthermore, the limiting dimensions of the pore "selectivity filter" for several cation-selective ion

Address correspondence to Richard D. Veenstra, Ph.D., Department of Pharmacology, SUNY Health Science Center at Syracuse, 750 East Adams Street, Syracuse, NY 13210. Fax: 315-464-8014.

[1]*Abbreviations used in this paper:* N2A, neuroblastoma; pdf, probability density function; rCx43, rat connexin43.

channels can be estimated using permeant organic cations (Hille, 1975; Dwyer et al., 1980; Hess et al., 1986).

In this report we examine the relative permeability of gap junction channels formed by rCx43 to monovalent cations and anions and determine the corresponding cationic and anionic conductance sequences using symmetrical equimolar ion substitutions and permeability sequences from ionic reversal potentials using asymmetrical solutions. The relative cation/lithium channel conductance and permeability ratios using both methods were in close agreement. Our data demonstrate that the rCx43 gap junction channel is permeable to all monovalent cations and anions tested. The relative conductance and permeability sequences are compared to models of (*a*) a diffusion-limited pore, (*b*) a restricted space-diffusion limited pore, and (*c*) a pore possessing electrostatic ion (binding)-site interactions within it. The relative selectivity sequence for the test ions closely resembled their relative aqueous mobilities with the exception of Rb^+ and Li^+, consistent with an Eisenman sequence II. The relative cation permeabilities in the presence of 136 mM chloride were determined by assuming $P_{Cl}/P_{Li} = 0.18$ as determined by asymmetric salt LiCl reversal potential experiments using raffinose and stachyose as impermeant sugars required to maintain the osmotic balance and electrochemical LiCl gradients. These permeability data predict an estimated pore radius of 6.3 ± 0.4 Å and a higher cation selectivity than previously reported for the rCx43 pore. A similar investigation of the rat connexin40 channel is reported in a second manuscript appearing in this issue (Beblo and Veenstra, 1997).

MATERIALS AND METHODS

Cell Culture and Transfection

Rat Cx43-transfected mouse N2A neuroblastoma cells (ATCC CCL131) were kindly provided by Dr. Eric C. Beyer (Washington University, St. Louis, MO). Connexin expression was verified by Northern blotting of total RNA prepared from selected clones (Veenstra et al., 1992). rCx43-transfected N2A cells were grown in minimal essential medium (GIBCO BRL, Gaithersburg, MD) supplemented with 10% heat-inactivated (56°C for 30 min) FCS (JRH Biosciences, Lenexa, KS), 1× nonessential amino acids, 2 mM L-glutamine, 0.5 mg/ml G418, 100 U/ml penicillin, and 100 U/ml streptomycin (GIBCO BRL).

Electrophysiological Recordings and Solutions

Connexin-transfected N2A cell cultures were plated at low density (2×10^5 cells/35 mm dish) for 24 h, washed with HEPES-buffered saline (in mM: 142 NaCl, 1.3 KCl, 0.8 $MgSO_4$, 0.9 NaH_2PO_4, 1.8 $CaCl_2$, 5 CsCl, 2 TEACl, 5.5 dextrose, and 10 HEPES, pH 7.2), and examined on the stage of an inverted phase-contrast light microscope (IMT-2; Olympus Corp., Lake Success, NY). rCx43-induced coupling in the transfected N2A cells was studied by double whole cell recording (DWCR) procedures as described previously (Veenstra and Brink, 1992). All holding potentials were controlled using the external and internal command inputs on the BioLogic RK-300 patch clamp amplifiers. Patch electrodes had resistances of 2-5 MΩ when filled with one of the nine test internal pipette solutions (IPS). The composition of each IPS is listed in Table I. The osmolarity of all bath and IPSs was measured by a freezing point osmometer (Model

TABLE I

Ionic Composition of Internal Pipette Solutions (IPS, mM)

Component, IPS:	KCl	NaCl	LiCl	RbCl	CsCl	TMACl	TEACl	TBACl	KBr	Kacetate	Kglutamate	Low LiCl
KCl	115	—	—	—	—	—	—	—	—	—	—	—
NaCl	—	115	—	—	—	—	—	—	—	—	—	—
LiCl	—	—	115	—	—	—	—	—	—	—	—	30
RbCl	—	—	—	115	—	—	—	—	—	—	—	—
CsCl	5	5	5	5	120	5	5	5	5	5	5	5
TMACl	—	—	—	—	—	115	—	—	—	—	—	—
TEACl	2	2	2	2	2	2	117	2	2	2	2	2
TBACl	—	—	—	—	—	—	—	115	—	—	—	—
KBr	—	—	—	—	—	—	—	—	115	—	—	—
Kacetate	—	—	—	—	—	—	—	—	—	115	—	—
Kglutamate	—	—	—	—	—	—	—	—	—	—	115	—
raffinose	—	—	—	—	—	—	—	—	—	—	—	169
KH_2PO_4	1	1	1	1	1	1	1	1	1	1	1	1
$M_gCl_2 \cdot 6H_2O$	4	4	4	4	4	4	4	4	4	4	4	4
$CaCl_2 \cdot 2H_2O$	3	3	3	3	3	3	3	3	3	3	3	3
BAPTA	5	5	5	5	5	5	5	5	5	5	5	3
HEPES	25	25	25	25	25	25	25	25	25	25	25	25
Na_2ATP	3	3	3	3	3	3	3	3	3	3	3	3
Na_2CP	3	3	3	3	3	3	3	3	3	3	3	3
osmolarity (mosm)	310	310	310	310	310	310	310	310	310	310	310	310
pH	7.0	7.0	7.0	7.0	7.0	7.0	7.0	7.0	7.0	7.0	7.0	7.0

3W2; Advanced Instruments Inc., Needham Heights, MA) and adjusted to 310 mosm. All experiments were performed at room temperature (20–22°C). For the channel conductance–mobility plots used to determine the relationship between differing cation and anion channel conductances and aqueous mobilities, we used the aqueous diffusion coefficient for the respective monovalent ion (D_{ion}) since D_{ion} is directly proportional to the aqueous mobility ($\mu_{ion} = (F/RT) \cdot D_{ion}$). D_{ion} (10^{-5} cm^2/s): Rb^+, 2.07; Cs^+, 2.06; K^+, 1.96; Na^+, 1.33; Li^+, 1.03; TMA^+, 1.19; TEA^+, 0.87; TBA^+, 0.52; Br^-, 2.08; Cl^-, 2.03; acetate$^-$, 1.09; and glutamate$^-$ (estimated), 0.36. The D_{ion} for glutamate was experimentally measured using two methods (see *Relative Ionic Permeability Calculations*).

Transjunctional potentials (V_j) were elicited by stepping the holding potential of the prejunctional cell (V_1) from a common holding potential ($V_1 = V_2 = 0$ mV, where V_2 is the holding potential of the postjunctional cell) to a new value (V'_1) for a minimum of 10 s. $V_j = V'_1 - V_2$ when the input resistances of cell 1 and cell 2 are 100-fold higher (e.g., 2 GΩ) than the resistances of the respective whole cell patch electrodes (e.g., 20 MΩ). Junctional current (I_j) was defined as the negative of the change in whole cell current of the postjunctional cell (ΔI_2). Errors in the $I_j = -\Delta I_2$ approximation are <2% when the input resistance of cell 2 and the junctional resistance are >2 GΩ and are 100-fold higher than the resistance of the recording electrode. The baseline $I_j = 0$ ($V_j = 0$) value, which varied by <1 pA during the course of each experiment, was monitored as an indicator of the stability of the I_j recordings. Note that the $I_j = 0$ baseline ≠ 0 pA in the whole cell recording since a small holding current (≤5 pA = I_2) must be applied at all times to hold the membrane potential of cell 2 constant at 0 mV. This nonjunctional current baseline must remain constant for the duration of all V_j pulses and is subtracted from the I_j measurements ($I_2 = [I_j = 0]$). Junctional currents are observed as simultaneous signals of equal amplitude and opposite polarity in both cells, although the whole cell current of cell 1 will contain nonjunctional membrane currents associated with the change in V_1 in addition to the I_j component ($\Delta I_1 = \Delta I_{m1} + I_j$, where ΔI_{m1} is the change in nonjunctional membrane current of cell 1 when $V_1 = V_2$ and I'_1 is the whole cell current during the V'_1 pulse). Junctional conductance (g_j) or resistance (R_j) was determined from the expression $g_j = 1/R_j = I_j/V_j$, provided that the above conditions are met. All current and voltage records were stored on VCR tape using a 4-channel digitizing unit (DR-484 Neuro-corder; Neuro Data Instruments Corp, NY, NY) and VCR tape recorder (Sansui SV-7700) for off-line analysis.

Channel Current Analysis

Junctional channel currents were displayed as paired whole cell currents or as individual ΔI_2 traces. All points current amplitude histograms were compiled from the $-\Delta I_2$ trace for each experiment. When recording single gap junction channel currents from a cell pair with γ_j <0.5 nS, $I_j \approx -\Delta I_2$ (Veenstra and Brink, 1992). We chose for channel analysis those cell pairs which exhibited the minimum number of active channels in each recording. The ground state ($I_j = 0$ pA) was identified by brief closures to the prepulse holding current for cell 2. All analog signals were low pass filtered (8-pole Bessel, LPF-30; WPI, Inc., Sarasota, FL) at 100 Hz and digitized at 2 kHz using a DT2801A A/D board (Data Translation, Inc., Marlboro, MA) installed in an IBM PC/AT clone (Everex 386SX/20) unless otherwise indicated. The dead time of the recording instrumentation was 1.8 ms. Off-line analysis of all digitized junctional current traces was performed using the DOSTAT program developed by Dr. S.V. Ramanan in the laboratory of Dr. P.R. Brink (Brink and Fan, 1989; Manivannan et al., 1992; Ramanan and Brink, 1993), and the methods are briefly described subsequently. The Gaussian distributions present in the all points current amplitude histogram were fitted with a probability density function (pdf):

$$f_I(M) = \sum_{n=0}^{M} B(M,n,p_1)\, f_b(I - I_n, \sigma_b^2 + n\sigma_o^2). \quad (1)$$

The binomial distribution:

$$B(M,n,p_1) = \frac{M!}{n!\,(M-n)!}\, p_1^n\, (1-p_1)^{M-n}, \quad (2)$$

assumes that there are M independent and identical channels with an open probability of p_1, of which n are open simultaneously. The current amplitude is determined by the difference in the mean current ($I - I_n$) between adjacent current peaks. The variance of the baseline and open channel noise are represented by σ_b^2 and σ_o^2. Since the area under each peak in an all-points amplitude histogram is equal to the cumulative open time of every n^{th} channel state, fitting the relative amplitudes of the peaks provides a direct estimate of the product of $M \times p_1$ for the observed channel activity (Brink and Fan, 1989; Manivannan et al., 1992; Ramanan and Brink, 1993). Event counts were generated by placing current crossing (threshold) detectors between adjacent peaks in the current amplitude histogram (≈1/2 amplitude) and the ΔI_2 trace was rescanned to count transitions with event durations ≥2 ms (4 digitized points). Channel mean open times were determined by dividing the sum of all open dwell times by the number of openings in each junctional current trace (Fenwick et al., 1982).

Relative Ionic Permeability Calculations

When asymmetrical 100:1 KCl/XCl or KCl/KY gradients were used to produce a nonzero reversal potential (E_{rev}) for the purpose of determining relative ionic permeabilities (P_X/P_K or P_{Cl}/P_{Li}), the following Goldman-Hodgkin-Katz voltage equation was used to calculate the ionic permeability terms for all of the monovalent ions present in the IPS:

$$E_{rev} = \frac{RT}{zF} 1n \left[\frac{P_K[K]_1 + P_{Cs}[Cs]_1 + P_{Na}[Na]_1 + P_{TEA}[TEA]_1}{P_K[K]_2 + P_{Cs}[Cs]_2 + P_{Na}[Na]_2 + P_{TEA}[TEA]_2} + \frac{P_{Cl}[Cl]_2 + P_X[X]_1 + P_Y[Y]_2}{P_{Cl}[Cl]_1 + P_X[X]_2 + P_Y[Y]_1} \right]. \quad (3)$$

A matrix was set up containing the concentrations for all of the monovalent cations and (135 mM Cl^-) and the experimentally measured E_{rev} for each set of asymmetric cationic substitution experiments including the LiCl/low LiCl+raffinose experiments and a single set of cationic and Cl^- permeability terms were generated which solved for all of the experimentally determined E_{rev}s (see Table V).

In all cases, Ag/AgCl wires were used for the bath ground and recording electrodes. The bath ground was placed in a separate reservoir filled with the same IPS LiCl or KCl used in one electrode during the asymmetric salt experiments. An agar salt bridge saturated with the external bath solution was used to connect the recording chamber to the ground reservoir. Hence, 136 mM Cl^- was present under all circumstances except for the patch electrode containing 115 mM KY (and only 22 mM Cl^- from the Cs^+, TEA^+, Ca^{2+}, and Mg^{2+} salts; Table I) during the asymmetric anion substitution experiments. Offset potentials were nullified in the bath using the junction potential potentiometer of the patch clamp amplifiers before GΩ seal formation and were not adjusted after the onset of whole cell recording. The values of these

junction potentials were tabulated and were negligible (≤2 mV) except when low Cl^- IPSs were used in one patch electrode. Hence, the E_{rev} values measured during the asymmetrical salt experiments are a consequence of the permeability differences of the ions through the rCx43 channel and do not reflect the differences in aqueous diffusion potentials for the different ionic compositions.

The D_{ion} for glutamate (relative to chloride) was estimated using the GHK voltage equation from measurements of the bath diffusion potential between an IPS KCl and IPS Kglutamate electrode which averaged 29.2 ± 0.8 mV. The diffusion potential of glutamate was also determined using double junction KCl electrodes (Ag/AgCl wire encased in 3 M KCl agar inside of a Pasteur pipette tip which was placed inside a 1 ml pipetteman tip also filled with 3 M KCl agar) and verified by similar diffusion potential measurements of several known anions (i.e., Br^-, Cl^-, $acetate^-$). Two double junction electrodes were used, one in the reference IPS KCl and the second in the IPS KY IPS (e.g., Kglutamate) with both leads connected to a voltmeter. An agar salt bridge (same as above) was used to connect the two solution chambers.

RESULTS

Cationic Unitary Channel Conductances

We measured the single channel current amplitudes of the rCx43 channel using internal pipette solutions containing 115 mM KCl (IPS KCl, Table I) or other monovalent cations. Fig. 1 *A* shows the double whole cell recording of a rCx43 channel in IPS KCl during a −50-mV transjunctional voltage (V_j) pulse. The current amplitude of each channel recording is obtained by fitting the all points (real time) histogram of the $-\Delta I_2$ trace with a probability density function (pdf, see MATERIALS AND METHODS) as illustrated in Fig. 1 *B*. To illustrate the symmetry of the rCx43 channel current amplitude with respect to V_j, the current recording and histogram of the same rCx43 channel obtained at +50 mV is also illustrated in Fig.1, *C* and *D*. Every current amplitude for each V_j is plotted in Fig. 1 *E* and the linear regression fit of the single rCx43 channel current-voltage relationship yielded a slope conductance (γ_j) for this cell pair of 100 pS ($r = 0.99$).

The IPS KCl single channel current-voltage relationships from three additional rCx43 cell pairs were determined using procedures identical to those described in Fig. 1. The γ_js from these individual i_j-V_j relations were 94.8, 95.1, and 96.9 pS and produced a mean γ_j value of 96.7 ± 2.3 pS for all four IPS KCl rCx43 experiments. When these four i_j-V_j relations were pooled together, linear regression analysis of the composite i_j-V_j relation produced a mean slope conductance (γ_j) of 96.9 pS (Fig. 2 *A*).

These procedures were repeated in rCx43 cell pairs with IPS RbCl, CsCl, NaCl, LiCl, TMACl, and TEACl. The pooled results from three rCx43 cell pairs using IPS RbCl are shown in Fig. 2 *B*, and the composite i_j-V_j relationship had a mean γ_j of 103.1 pS, again comparable to the mean γ_j of 101.3 ± 3.0 pS determined from the independent slope conductances of the three IPS RbCl rCx43 experiments (98.0, 103.0, and 103.1 pS). Three independent rCx43 channel experiments in IPS CsCl had slope conductances of 102.2, 103.3, and 107.1 pS for a mean γ_j of 104 ± 2.8 pS. The composite i_j-V_j relationship for IPS CsCl shown in Fig. 2 *C* had a mean γ_j of 101.7 pS. The slope conductances of seven IPS NaCl rCx43 cell pairs were 74.0, 75.1, 76.3, 78.3, 79.7, 80.7, and 81.3 pS, which gives a mean γ_j of 77.9 ± 2.8 pS. The composite i_j-V_j relationship for IPS NaCl shown in Fig. 2 *D* had a similar mean γ_j of 78.8 pS. The fifth alkali metal cation we examined was LiCl, and four independent determinations of the linear slope conductance in IPS LiCl were 74.9, 76.1, 77.3, and 77.9 pS, which gives a mean γ_j of 76.6 ± 1.3 pS. Again, the mean γ_j of the composite i_j-V_j relationship for IPS LiCl was similar at 78.2 pS (Fig. 2 *E*). IPS TMACl produced a mean γ_j of 65.0 ± 3.0 pS as determined from three independent experiments. The composite i_j-V_j relationship for IPS TMACl shown in Fig. 2 *F* had an identical mean γ_j of 64.9 pS. Four rCx43 channel recordings were obtained in IPS TEACl and the mean slope conductances were 51.4, 51.6, 54.8, and 54.8 pS, which gives a mean γ_j of 53.2 ± 1.9 pS. The composite i_j-V_j relationship for IPS TEACl shown in Fig. 2 *G* had a similar mean γ_j of 53.0 pS. The largest organic cation we tested, TBACl, produced less stable channel recordings than the other monovalent cations examined, and only two to four V_j pulses could be applied to each cell pair. Hence, individual i_j-V_j relationships were not obtained for all four cell pairs examined. Our best γ_j estimate of the rCx43 channel in TBACl is 37 pS based on only four negative V_j pulses from a single cell pair (data not shown).

Each V_j pulse had a minimum duration of 2 min, and the amplitudes of all stable channel current levels were plotted as indicated in the respective i_j-V_j relationships illustrated in Fig. 2. Although the channel amplitude, variance, and open probabilities are determined by calculating a best fit probability density function for independent channels and are, therefore, independent of event count determinations, Table II summarizes the total event counts at each V_j for the rCx43 channels observed in each of the IPSs.

Relationship between Channel Conductance and Cationic Aqueous Mobility

The cation conductance sequence based on the maximum single channel conductance state of the rCx43 channel in each of the IPSs was $Cs^+ \geq Rb^+ > K^+ > Na^+ \geq Li^+ > TMA^+ > TEA^+$. This ordering does not correspond exactly with their known ionic aqueous mobility sequence. According to their aqueous mobilities, we would expect the rCx43 channel conductance in the presence of Li^+ to be 20% lower than in the presence of Na^+ and Rb^+ to be slightly higher in conduc-

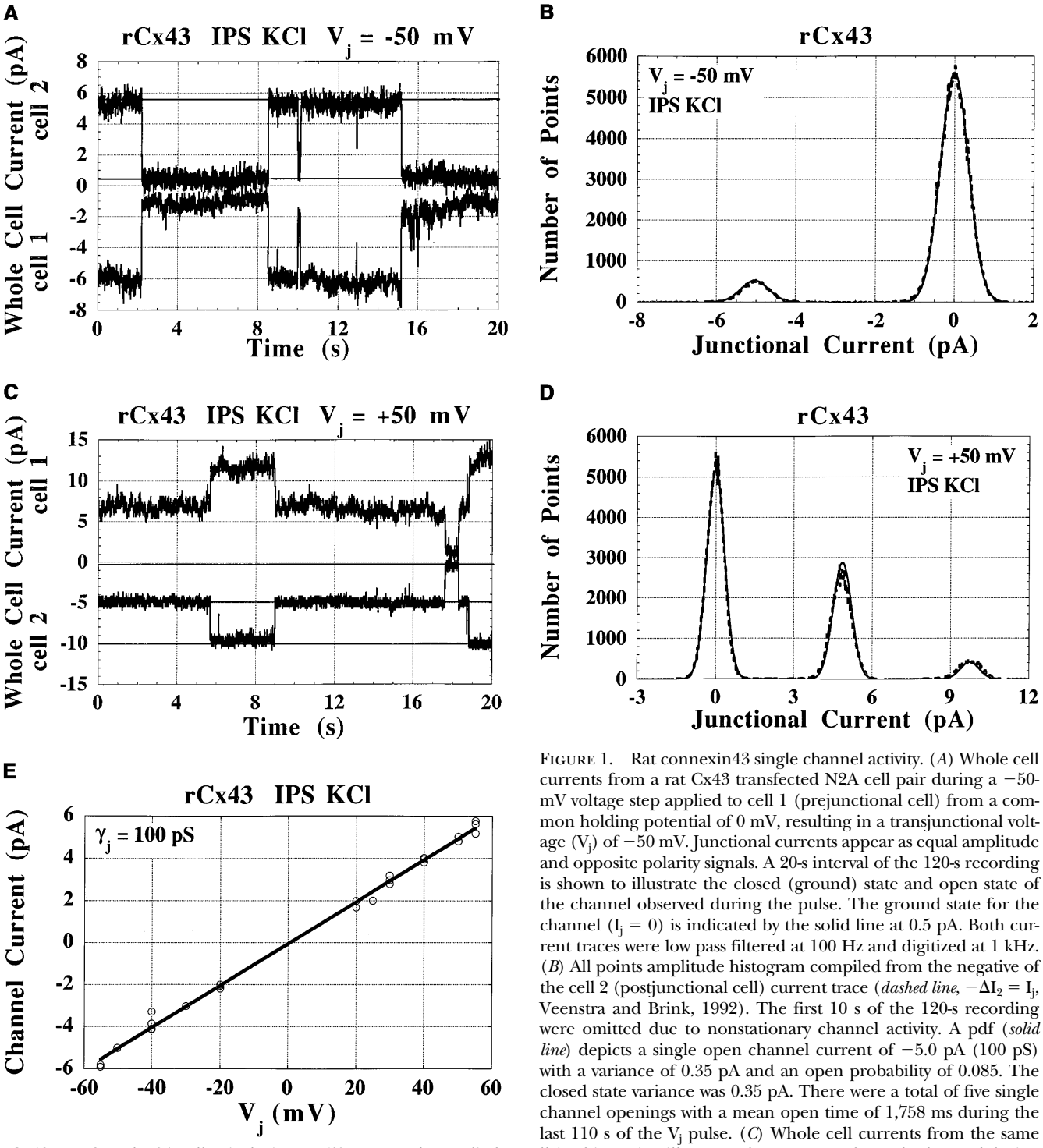

FIGURE 1. Rat connexin43 single channel activity. (*A*) Whole cell currents from a rat Cx43 transfected N2A cell pair during a −50-mV voltage step applied to cell 1 (prejunctional cell) from a common holding potential of 0 mV, resulting in a transjunctional voltage (V_j) of −50 mV. Junctional currents appear as equal amplitude and opposite polarity signals. A 20-s interval of the 120-s recording is shown to illustrate the closed (ground) state and open state of the channel observed during the pulse. The ground state for the channel ($I_j = 0$) is indicated by the solid line at 0.5 pA. Both current traces were low pass filtered at 100 Hz and digitized at 1 kHz. (*B*) All points amplitude histogram compiled from the negative of the cell 2 (postjunctional cell) current trace (*dashed line*, $-\Delta I_2 = I_j$, Veenstra and Brink, 1992). The first 10 s of the 120-s recording were omitted due to nonstationary channel activity. A pdf (*solid line*) depicts a single open channel current of −5.0 pA (100 pS) with a variance of 0.35 pA and an open probability of 0.085. The closed state variance was 0.35 pA. There were a total of five single channel openings with a mean open time of 1,758 ms during the last 110 s of the V_j pulse. (*C*) Whole cell currents from the same rCx43 transfected N2A cell pair during a +50-mV V_j pulse applied to cell 1. This tracing illustrates the two open channels observed during this 150 s V_j pulse. The closed state is indicated by the solid line at −0.3 pA. Both current traces were low pass filtered at 100 Hz and digitized at 1 kHz. (*D*) All points amplitude histogram of the $-\Delta I_2$ current trace (*dashed line*) and calculated pdf (*solid line*) depicting two channels with current amplitudes of 4.8 and 4.95, open channel variance of 0.25 pA, and open probabilities of 0.25 and 0.20. The closed state variance was 0.24 pA. There were a total of 21 channel openings with a mean open time of 3,371 ms. (*E*) Single channel current-voltage relationship for the rCx43 cell pair illustrated in this figure. Each symbol represents the measured current amplitude of an observed channel for a given V_j pulse. The single channel slope conductance (γ_j) of 100 pS was determined from the linear regression fit (*solid line*) of the data ($r = 0.99$).

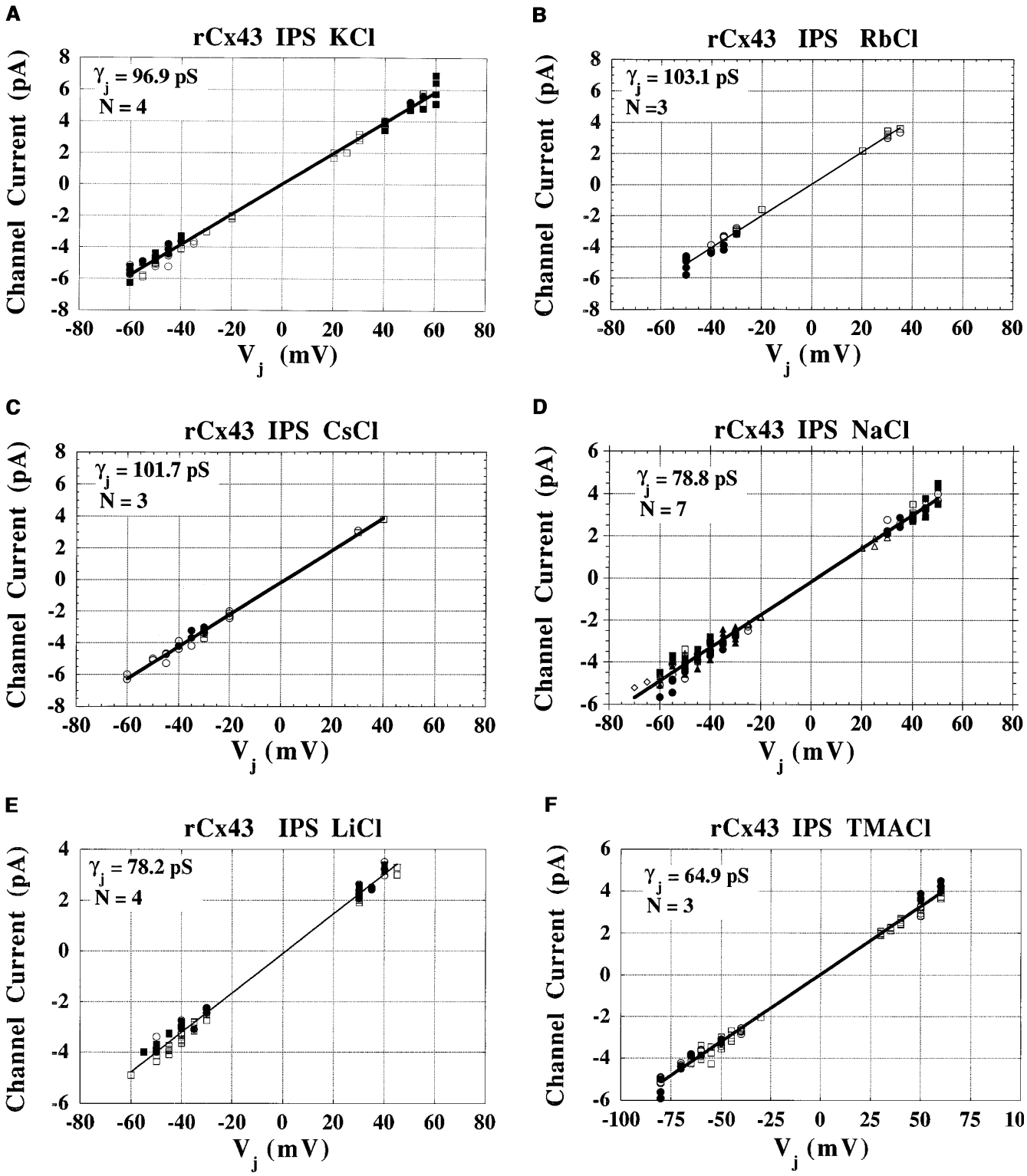

FIGURE 2

tance than Cs^+. These results are consistent with the hypothesis that the rCx43 channel possesses a weak electrostatic field site associated with the pore, as proposed by Veenstra et al. (1995). Since the commonly accepted interpretation of a gap junction channel assumes that channel conductance is limited by aqueous diffusion, we chose to examine the single channel conductances (γ_{XCl}) as a function of the aqueous mobility for each

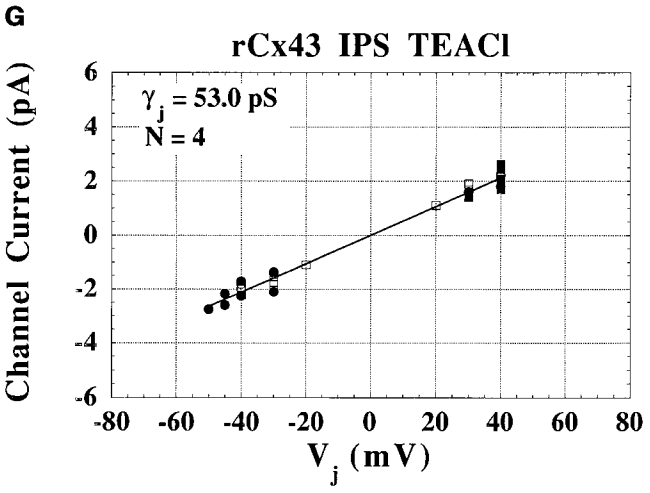

FIGURE 2. Cationic single channel junctional current-voltage relationships. (*A*) Linear regression fit (*solid line*) of the single channel current amplitudes obtained at the respective transjunctional voltage in IPS KCl. Each symbol type refers to a different experiment ($n = 4$) and every current amplitude was obtained using the procedures illustrated in Fig. 1. The slope conductance is 96.9 pS. (*B*) The same for three experiments in IPS RbCl. The slope conductance was 103.1 pS. (*C*) The single channel current-voltage relationship for three cell pairs in IPS CsCl with a slope of 101.7 pS. (*D*) The single channel current-voltage relationship for seven cell pairs in IPS NaCl with a slope of 78.8 pS. (*E*) The single channel current-voltage relationship for four cell pairs in IPS LiCl with a slope of 78.2 pS. (*F*) The single channel current-voltage relationship for three cell pairs in IPS TMACl with a slope of 64.9 pS. (*G*) The single channel current-voltage relationship for four cell pairs in IPS TEACl with a slope of 53.0 pS. The slope conductances illustrated here are not statistically different from the mean γ_j calculated from the individual single channel junctional current-voltage relationships for each cation (see RESULTS). Correlation coefficients were >0.99 for all graphs.

cation. The smallest diameter atomic monovalent cation (Li^+) has the largest energy of hydration, consistent with its known aqueous mobility relative to the other alkali metal ions, while the organic tetraalkylammonium monovalent cations possess an increasing molecular diameter and decreasing hydration energy. Hence, the hydration energy and size of the permeant ion are both variables which limit the observed rCx43 channel conductance for a particular ion. The experimentally determined γ_{XCl} values are plotted as a function of aqueous mobility in Fig. 3 *A*. The channel conductance-mobility plot (γ_j-μ) for the test cations approximates a linear function. This plot also predicts a minimum anionic (Cl^-) γ_j of 29.5 pS in the presence of an immobile (impermeant) cation for the rCx43 channel under the ionic conditions used for these experiments (see Table I). A similar plot for the test anions (see Fig. 5 *A*) can be used to make similar predictions about the minimum cationic (primarily K^+) γ_j of 51.2 pS in the presence of an immobile (impermeant) anion for the rCx43 channel under these experimental ionic conditions. Since the sum of the two minimum γ_js does not equal the γ_j of 96.9 pS observed in 115 mM KCl, we hypothesized that the mobility of the ions in the pore is reduced relative to their mobilities in bulk solution due to frictional (solvent) drag within the pore.

To model this effect, we used the derivation of Levitt (1991) which approximates the diffusion coefficient at site x (D_x) in the channel relative to the bulk solution (D_o) in terms of the radius of a spherical ion relative to the radius of the channel at site x.

$$\frac{D_x}{D_o} = \frac{(1 - 2.1054\lambda + 2.0805\lambda^3 - 1.7068\lambda^5 + 0.72603\lambda^6)}{(1 - 0.75857\lambda^5)}, \quad (4)$$

where λ = the ratio of unhydrated ionic radius/pore radius. Pore radius was assumed to be constant for the entire length of the pore for these calculations. The output of this equation models only the effect of ionic/pore radii on the aqueous mobility for each ion. This equation also predicts that $D_x \leq 0.05D_o$ when $\lambda \geq 0.70$. Assuming various pore radii, D_x/D_o was calculated for the test ions and linear plots of γ_j vs. pore radius were then determined until an exact solution could be found

TABLE II

Cumulative Event Counts for Cation Single Channel Current-Voltage Relationships

IPS V_j =	−80	−70	−65	−60	−55	−50	−45	−40	−35	−30	−25	−20	20	25	30	35	40	45	50	55	60
KCl	—	—	—	846	514	124	112	169	125	27	—	69	356	—	29	—	237	—	99	54	96
NaCl	—	68	2	389	59	897	886	849	530	291	93	26	23	382	758	55	431	125	250	—	107
LiCl	—	—	—	89	328	543	360	537	627	434	—	—	—	—	254	122	196	—	28	—	—
RbCl	—	—	—	—	—	286	—	278	137	182	—	123	26	—	158	118	—	—	—	—	—
CsCl	—	—	—	20	—	426	245	235	510	548	—	356	—	—	109	—	57	—	—	—	—
TMA	120	193	294	934	121	789	54	381	126	159	—	—	—	—	34	110	81	—	179	—	36
TEA	—	—	—	—	—	—	22	362	—	633	—	377	514	—	1719	—	933	—	—	—	—
KBr	—	42	8	517	—	76	255	759	8	251	—	6	172	—	490	39	317	—	—	—	—
Kac	—	—	—	232	—	491	—	507	—	935	—	—	—	—	981	—	—	—	779	—	—
Kgl	—	93	879	907	585	1176	295	1446	15	438	397	—	—	—	159	667	1099	580	164	281	331

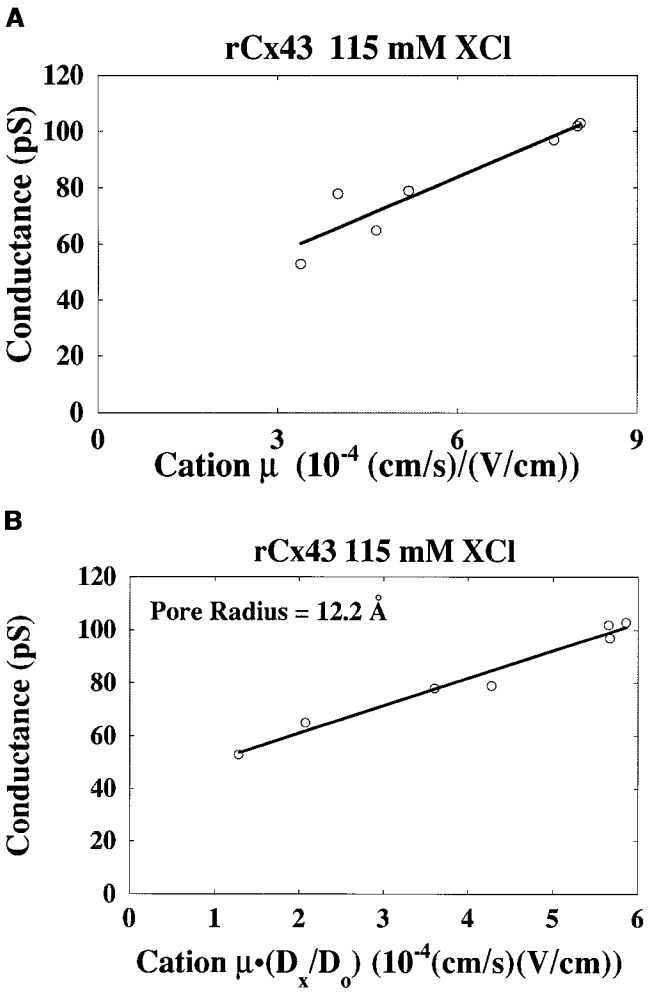

FIGURE 3. Unitary conductances of the rCx43 channel in the presence of the test inorganic and organic cations illustrated in Fig. 2. (*A*) The rCx43 single channel conductance is plotted as a function of the aqueous mobility (μ) of the respective ion ($TEA^+ < TMA^+ < Li^+ < Na^+ < K^+ < Rb^+ < Cs^+$). The experimental data is represented by the open circles and the solid line is a linear regression fit of the data with a y-intercept of 29.49 pS and a slope of 9.05 pS/([cm/s]/[V/cm]) ($r > 0.94$). (*B*) A similar plot of the cation conductance-mobility after scaling μ for each ion by a factor D_x/D_o determined by the ratio of the ionic radius to an estimated pore radius of 12.2 Å. The experimental data is represented by the open circles and the solid line is a linear regression fit of the data with a y-intercept of 40.49 pS and a slope of 10.33 pS/([cm/s]/[V/cm]) ($r > 0.97$).

for the rCx43 channel in 115 mM KCl. The resulting plot is shown in Fig. 3 *B* and predicts a minimum anionic γ_j of 40.5 pS and a pore radius of 12.2 Å. Tables III and IV summarize the physical parameters of the various ions and the summary statistics of the linear regression fits of the channel conductance-mobility · (D_x/D_o) plots.

Anionic Unitary Channel Conductances

Equimolar ion substitution of three different anions (Table I) for chloride were also performed using identical procedures to those described above for the seven cations. The composite i_j-V_j relationship for four cell pairs in IPS KBr is shown in Fig. 4 *A* and had a slope conductance of 104.9 pS. This is similar to the mean γ_j of 105.7 ± 3.3 pS calculated from the slope conductances of the four individual experiments (102.9, 104.4, 104.9, 110.5 pS). Four rCx43 experiments with IPS Kacetate produced linear single channel i_j-V_j relationships with slope conductances of 76.0, 76.3, 77.0, and 84.2 pS, or a mean γ_j of 78.4 ± 3.9 pS. The IPS Kacetate composite i_j-V_j relationship had a slope conductance of 76.8 pS (Fig. 4 *B*). The largest organic anion tested was glutamate and four experiments with IPS Kglutamate yielded a mean γ_j of 61.5 ± 1.7 pS (59.6, 60.9, 62.3, and 62.6 pS). The IPS Kglutamate i_j - V_j relationship had a slope conductance of 61.0 pS (Fig. 4 *C*). Table II again summarizes the total event counts at each V_j for the rCx43 channels observed in each of the IPSs.

Relationship between Channel Conductance and Anionic Aqueous Mobility

The anion selectivity sequence based on the maximum single channel conductance state of the rCx43 channel in each of the IPSs was $Br^- > Cl^- >$ acetate$^-$ >

TABLE III

Physical Constants Used for Channel Conductance-Mobility Plots

Ion	γ_j	Radius	Mobility
	*p*S	*Å*	*10^{-4} (cm/s)(V/cm)*
Rb	103	1.61	8.09
Cs	102	1.74	8.01
K	97	1.51	7.62
Na	79	1.02	5.19
Li	78	0.59	4.01
TMA	65	3.47	4.65
TEA	53	4.00	3.39
Br	105	1.96	8.09
Cl	97	1.81	7.92
Acetate	77	2.90	4.24
Glutamate	61	3.15	2.73

TABLE IV

Estimation of Pore Size by Linear Regression of Modified γ_j–μ Plots

Parameter	Pore Size					
Cation	8 Å	10 Å	12 Å	12.1 Å	12.2 Å	15 Å
y-intercept (pS)	48.02	43.80	40.78	40.62	40.49	37.66
Slope	10.53	10.41	10.34	10.33	10.33	10.23
r	0.95	0.97	0.98	0.99	0.99	0.99
Anion	8 Å	10 Å	12 Å	12.1 Å	12.2 Å	15 Å
y-intercept (pS)	59.68	57.80	56.55	56.50	56.45	55.33
Slope	9.82	8.82	8.25	8.23	8.22	7.76
r	0.97	0.98	0.98	0.98	0.98	0.98

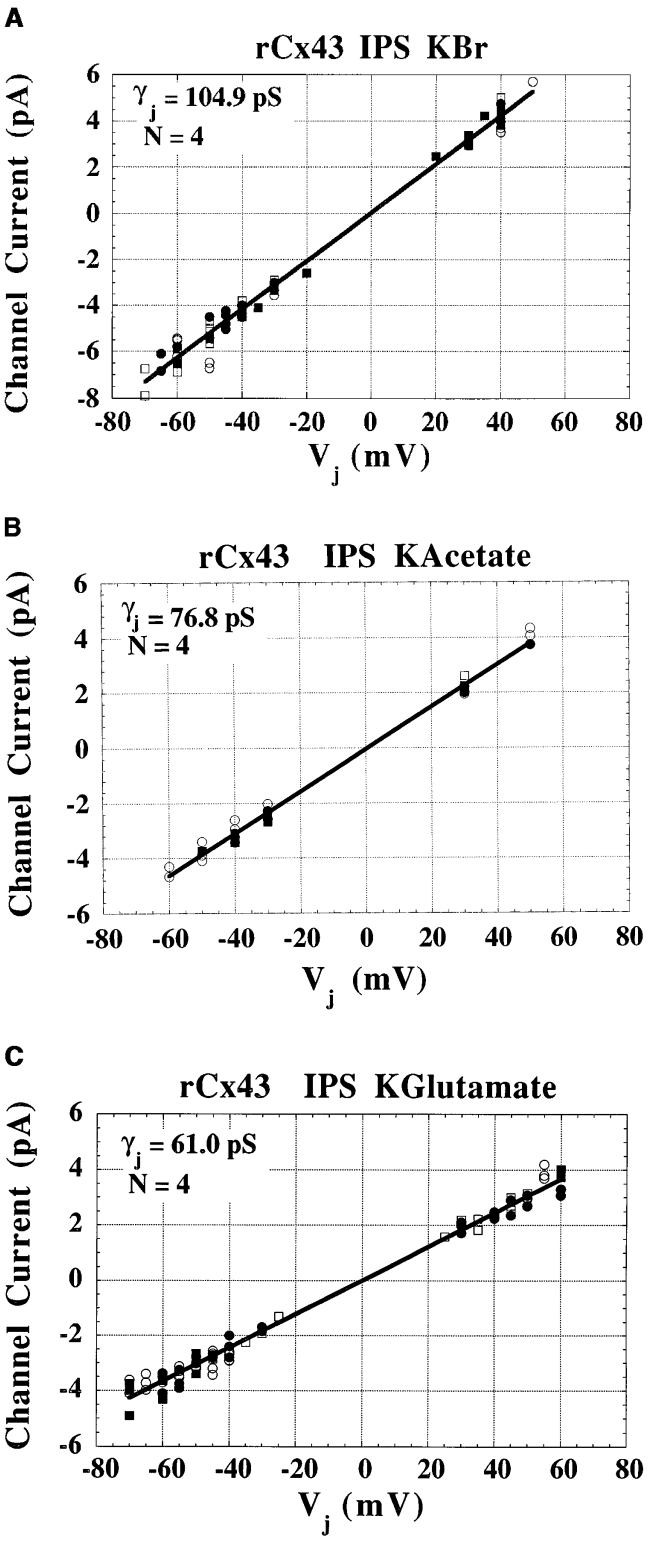

FIGURE 4. Anionic single channel junctional current-voltage relationships. (*A*) Linear regression fit (*solid line*) of the single channel current amplitudes obtained at the respective transjunctional voltage in 115 mM KBr. Each symbol type refers to a different experiment ($n = 4$) and every current amplitude was obtained using the same procedures illustrated for the cations examined above. The slope conductance is 104.9 pS. (*B*) The single channel current-voltage relationship for four cell pairs in 115 mM Kacetate with a slope of 76.8 pS. (*C*) The single channel current-voltage relationship for four cell pairs in 115 mM Kglutamate with a slope of 61.0 pS. The slope conductances illustrated here are not statistically different from the mean γ_j calculated from the individual single channel junctional current-voltage relationships for each cation (see RESULTS). Correlation coefficients were >0.99 for all graphs.

glutamate$^-$. Since this sequence is consistent with an aqueous mobility sequence for the test anions, these results are indicative of a weak or nonexistent cationic electrostatic site within the pore of the rCx43 channel. The experimentally determined γ_{KY} values are plotted as a function of aqueous mobility in Fig. 5 *A*. As with the cations, the data illustrate that the γ_js and aqueous mobilities (μ) of the test anions approximates a linear function, again indicative of an aqueous pore. This plot also predicts a minimum cationic (K^+) γ_j of 51.2 pS in the presence of an immobile (impermeant) anion for the rCx43 channel under the present ionic conditions. To account for the reduction in aqueous mobility within the pore according to the factor D_x/D_o, linear plots of γ_j vs pore radius for the test anions were determined. The resulting plot for a pore with a radius of 12.2 Å is shown in Fig. 5 *B* and predicts a minimum cationic γ_j of 56.5 pS.

Relative Cation Permeability Ratios and Estimates of Pore Size

The rCx43 channel conductance sequence and pore diameter estimates provided thus far are based on models for an aqueous diffusion limited pore. To further examine the ionic selectivity and pore diameter, asymmetric salt reversal potential experiments were performed on the monovalent cations and anions listed in Table I. For the cations, all reversal potentials were performed relative to Li^+ since the mean γ_j in IPS LiCl demonstrated the greatest deviation from an Eisenman I aqueous mobility sequence (compared to Na^+ and TMA^+) of all of the cations tested. For all cationic asymmetric salt experiments, the Nernst potential for Li^+ was −116 mV and the opposing Nernst potential for the counterpart cation was +116 mV (oppositely directed 100:1 concentration gradients, 1.2 mM of each major cation was added to the opposite side). The equilibrium potential for all other permeant ions (symmetrical concentrations of Cl^- and all other cations) was 0 mV. Fig. 6 *A* illustrates the i_j-V_j relationship obtained from three experiments using IPS KCl/LiCl. The measured reversal potential (E_{rev}) was +5.4 mV and is in close agreement with the mean E_{rev} of 5.5 ± 0.1 mV determined from the E_{rev} of each of the four experiments. The E_{rev} was determined for each of the cations using the identical protocol to the one illustrated here and the results are summarized in Table V. Since the cationic E_{rev}s were all obtained in the presence of 136 mM

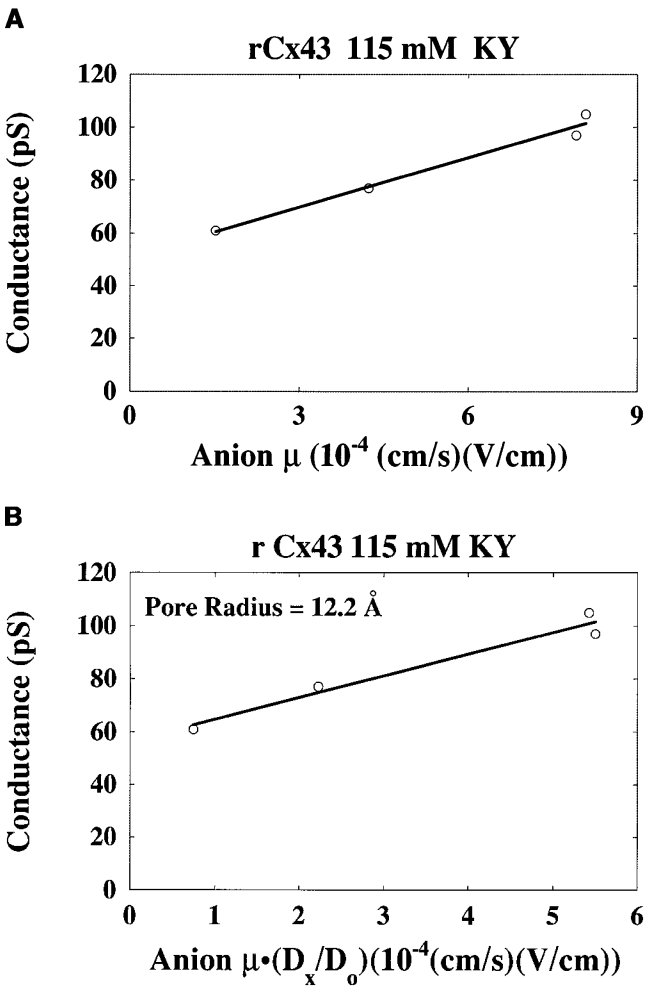

FIGURE 5. Unitary conductances of the rCx43 channel in the presence of the test inorganic and organic anions illustrated in Figs. 4 and 5. (*A*) The rCx43 single channel conductance is plotted as a function of the aqueous mobility (μ) of the respective ion ($glutamate^- < acetate^- < Cl^- < Br^-$). The experimental data is represented by the open circles and the solid line is a linear regression fit of the data with a y-intercept of 51.15 pS and a slope of 6.22 pS/([cm/s]/[V/cm]) ($r > 0.98$). (*B*) A similar plot of the anion conductance-mobility after scaling μ for each ion by a factor D_x/D_o determined by the ratio of the ionic radius to an estimated pore radius of 12.2 Å. The experimental data is represented by the open circles and the solid line is a linear regression fit of the data with a y-intercept of 56.45 pS and a slope of 8.22 pS/([cm/s]/[V/cm]) ($r > 0.98$).

Cl^- in addition to the small amounts of Cs^+, TEA^+, and Na^+ found in each IPS, the relative permeability terms could not be directly determined using the biionic equation. Instead, the Goldman-Hodgkin-Katz voltage equation containing all of the monovalent ions was used to calculate the cationic E_{rev}s shown in Table V (see MATERIALS AND METHODS, *Relative Ionic Permeability Calculations*). Critical to these determinations was the relative permeability value of Cl^- with respect to the cations which could not be directly assessed from these cationic asymmetric salt reversal potential experiments.

To directly assess the permeability of Cl^- relative to Li^+, we established an asymmetric 115:30 mM LiCl gradient between the two rCx43 transfected cells using the tri- and tetrasaccharides raffinose and stachyose to maintain osmotic balance (169 mM). The resulting i_j-V_j relationship from the seven 115 mM LiCl:30 mM LiCl + 169 mM raffinose experiments is shown in Fig. 6 *B*. The low LiCl IPS still contained the usual amount of Cs^+, Na^+, and TEA^+ as listed in Table I. Calculated Nernst potentials for Li^+ and Cl^- were −33.9 and 24.8 mV respectively. The measured E_{rev} was −16.5 mV (mean E_{rev} ± SD = −16.3 ± 1.0 mV). A nearly identical E_{rev} of −16.27 mV was obtained from one experiment using stachyose instead of raffinose. This E_{rev} was used in the GHK voltage equation to simultaneously solve for the relative permeabilities of all cations and chloride relative to Li^+ as indicated in Table V. The experimentally measured and calculated (GHK) E_{rev}s are indicated for all asymmetric cation solutions tested, and this one set of relative permeabilities satisfies all of the experimental conditions examined. The relative permeability of Na^+ is only 5% higher than that of Li^+ and the relative permeability of TMA is 26% lower than Li^+, in close agreement with the conductance ratios obtained using symmetrical solutions as shown in Fig. 2. These results also demonstrate that the permeability of Rb^+ is higher than that of Cs^+, consistent with an Eisenman II sequence. The results also fix the relative Cl^- permeability to be only 18% relative to Li^+ or 13% relative to K^+, lower than the estimated $P_{Cl/K}$ of 0.71 based on the diffusion limited models presented in Figs. 3 and 5.

The relative permeability ratios of permeant cations has frequently been used to provide an estimate of the pore radius using the hydrodynamic equation (Dwyer et al., 1980):

$$\frac{P_X}{P_{Li}} = C \cdot (1-\alpha^2) \cdot \frac{(1 - 2.105\alpha + 2.0865\alpha^3 - 1.7068\alpha^5 + 0.72603\alpha^6)}{(1 - 0.75857\alpha^5)}, \quad (5)$$

where α is the radius ratio of a cylinder with radius r permeated by spherical ions of radius a and *C* is a constant used to calculate the area at the mouth of the pore. The resulting plot is illustrated in Fig. 6 *C* and depicts the relationship between the cation relative permeability values (*filled circles*) and their hydrated radius (Nightingale, 1959). The solid line represents the theoretical fit of the data determined from the above equation assuming a pore radius of 6.3 ± 0.4 Å and $C = 45.8$ (mean ± standard error of pore radius determined by Chi-squared fit of data).

Asymmetric salt reversal potential experiments were

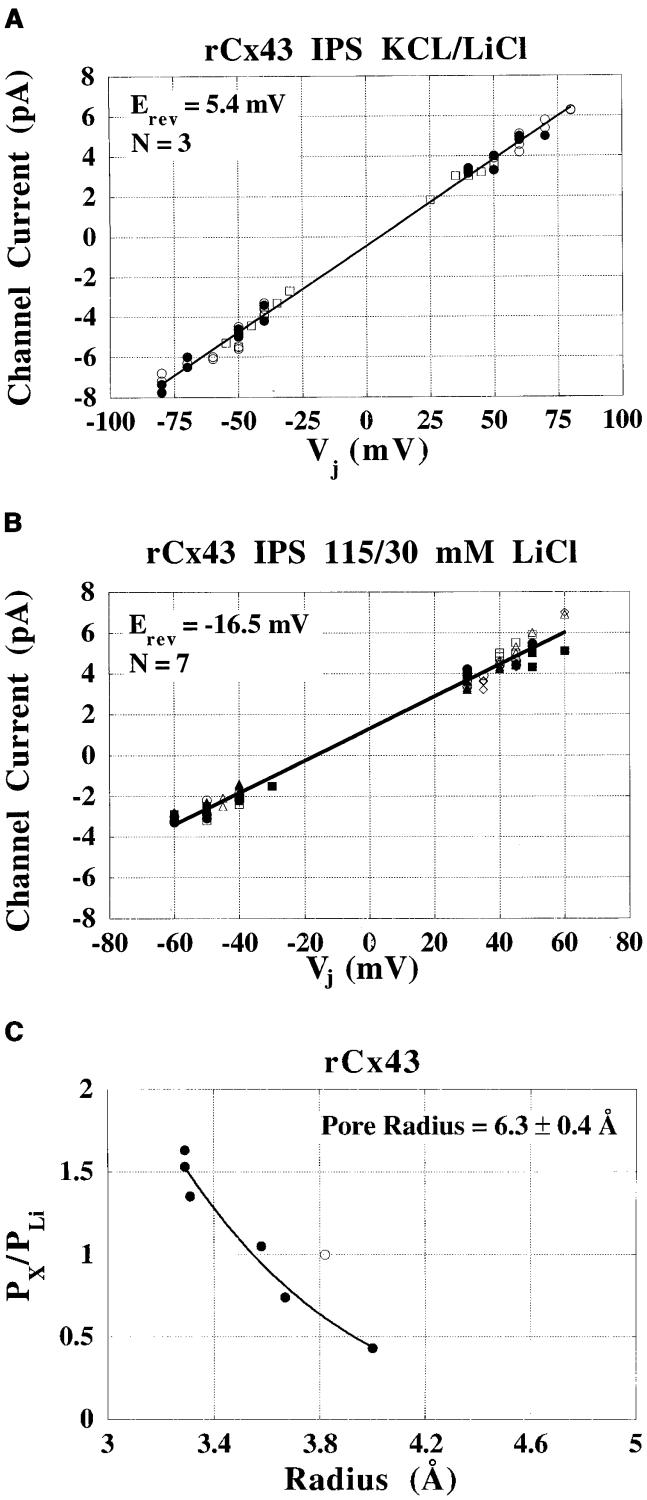

FIGURE 6. Relative permeability and pore radius of the rCx43 channel. (*A*) Asymmetric salt reversal potential experiments using IPS KCl and LiCl were performed using the same voltage protocols as described in Figs. 1, 2, and 4. Each symbol represents a different experiment and the data points represent the channel amplitudes obtained at the respective V_j from three rCx43 cell pairs. The solid line is a linear regression fit of the data ($r > 0.99$) indicating a reversal potential of 5.4 mV (KCl cell negative) which was used to calculate the relative P_K/P_{Li} permeability ratio listed in Table V. (*B*) Another composite i_j-V_j relationship this time using an asymmetric LiCl gradient of 115/30 mM with 169 mM raffinose added unilaterally to maintain the osmotic balance between the two cells. The linear regression fit indicates a reversal potential of −16.5 mV (115 mM LiCl cell negative, $r > 0.99$) which was used to calculate the relative P_{Cl}/P_{Li} permeability ratio listed in Table V. (*C*) Estimation of the rCx43 pore radius as determined from the relative permeability and hydrated radii of the permeant cations. The relative P_X/P_{Li} values (*filled circles*, *open circle* = P_{Li} = 1.0) from Table V are plotted relative to their hydrated radii (Nightingale, 1959). The solid line is a Chi-squared fit (r = 0.98) of the filled circles using the hydrodynamic equation (see text) which accounts for the excluded volume at the mouth of the channel by an ion with radius a and a frictional drag coefficient based on the relative radius of the ion to the radius r of a right cylindrical pore which was assumed to be 6.3 ± 0.4 Å.

also performed for the anions in the presence of a symmetrical 116 mM K^+ gradient (Cs^+, Na^+, and TEA^+ were also present in their usual amounts). The reversal potentials for Br^-, acetate$^-$, and glutamate$^-$ relative to Cl^- followed the same order as the channel conductance sequence (data not shown). These results are consistent with the aqueous mobility sequence (lyotropic or Eisenman I sequence) for the test monovalent anions. However, the experimentally measured anionic reversal potentials could not be calculated using the Goldman-Hodgkin-Katz voltage equation, taking into account the P_K/P_{Cl} of 7.5 as determined from Table V. This is not entirely unexpected for a channel that is permeable to both monovalent cations and anions as reported for other ion channels (see DISCUSSION; Borisova et al., 1986; Zambrowicz and Colombini, 1993; Franciolini and Nonner, 1994). This implies that the assumption of ionic independence inherent to the constant field equation is not valid for the rCx43 channel. Further determination of the mechanisms for anion and cation permeability will require additional experimentation.

For all of the asymmetric ionic solution experiments, it is imperative that the transjunctional voltage (V_j) be defined in a consistent manner. In the double whole cell configuration, V_j is the difference between the holding potentials of the two cells ($V_j = V_{cell1} - V_{cell2}$ or vice versa). In constructing an I-V curve, we typically define cell 1 as the prejunctional cell which receives the ΔV command pulse while cell 2 is held at a constant potential. This convention is of little consequence when symmetrical salt solutions are used, but is very important when ionic reversal potentials such as those reported in Table V are to be determined. Hence, as mentioned above, even when voltage pulses are applied alternatively to both cells, V_j is still defined relative to one cell (e.g., the KCl-containing cell as in the KCl/LiCl experiments mentioned above). Otherwise, the current amplitudes obtained when pulsing the LiCl cell

TABLE V

Relative Cation Permeability Coefficients Determined from Asymmetric Salt Reversal Potentials

Ion	N	Mean E_{rev} ± SD	Measured E_{rev}	P_{ion}	Calculated E_{rev}	Relative γ_j ratio
		mV	*mV*		*mV*	
Rb^+	4	9.5 ± 1.3	+9.2	1.63	+9.2	1.32
Cs^+	4	8.6 ± 0.7	+7.9	1.53	+7.9	1.30
K^+	3	5.5 ± 0.1	+5.4	1.35	+5.5	1.24
Na^+	2	1.2 ± 0.1	+0.8	1.05	+0.8	1.01
Li^+	—	—	—	1.0	—	1.0
TMA^+	3	−4.9 ± 0.9	−5.0	0.74	−5.0	0.83
TEA^+	5	−12.7 ± 0.7	−12.7	0.43	−12.8	0.68
*LiCl/raffinose + LiCl	7	−16.3 ± 1.0	−16.5	0.18	−16.3	—

N, number of cell pairs. Mean E_{rev} ± SD, statistical mean ± SD from N experiments. Measured E_{rev}, value obtained from composite i_j-V_j relationship of N experiments. Calculated E_{rev}, product of GHK voltage equation calculations for all monovalent cations and Cl^-. Relative γ_j ratio, channel conductance ratios determined from symmetrical solutions (Fig. 2). *Cl^- relative permeability was determined using IPS LiCl in one pipette and low (30 mM) LiCl +169 mM raffinose IPS in the other pipette.

will be transposed on the voltage axis relative to the data obtained when pulsing the KCl cell. A linear I-V relation is not expected for asymmetric ionic solutions, depending on the relative differences in the permeabilities of the two opposed ions. Large deviations from linearity are expected when using two ions with drastically different permeabilities, which are minimized here by using Li^+ since its conductance was near the midpoint for all of the cations examined. Li^+ was primarily chosen because its conductance deviated most from the known monovalent cation aqueous mobility sequence.

DISCUSSION

The purpose of this investigation was to determine the relative monovalent cation and anion permeability sequences of the rCx43 channel. We then compared them to the known Eisenman sequences in order to approximate the relative electrostatic field strength of an interacting binding site for the partially hydrated ions within the pore. The results presented in Figs. 2 and 3 confirm the monovalent cation conductance sequence of the maximum conductance state of the rCx43 channel to be $Rb^+ \geq Cs^+ > K^+ > Na^+ \geq Li^+ > TMA^+ > TEA^+$. This conductance sequence is consistent with an aqueous mobility sequence with some quantitative differences, the $Rb^+ \approx Cs^+$ and $Li^+ \approx Na^+$ conductances are statistically indistinguishable, which suggests that aqueous mobilities are being altered in a disproportionate manner for some cations relative to others. Two possible mechanisms include binding (which relates to energy required for dehydration of an ion) and physical size limitations (solvent drag or exclusion based on ionic/pore diameters). We have attempted to address both mechanisms in the present investigation. The binding energy of an ion for a site cannot be calculated without determining its dissociation constant (K_d) which was not performed here since we had no prior indication of potential binding sites within connexin channels. Comparison of the conductance ratio sequence to the relative permeability sequence confirms the above selectivity sequence for the cations and establishes the relative permeability of Rb^+ to be slightly greater than Cs^+, which corresponds to an Eisenman II sequence (Eisenman and Horn, 1983).

The anionic conductance sequence was determined to be $Br^- > Cl^- >$ acetate$^-$ > glutamate$^-$, which matches the aqueous mobility sequence for these four monovalent anions. These findings imply that the rCx43 pore has a low affinity for the various monovalent ions examined, consistent with their permeation through an aqueous pore containing a weak anionic electrostatic field which only partially dehydrates the permeant cations. The relative anion-to-cation permeability of the rCx43 channel was also determined by creating an asymmetric salt reversal potential for LiCl using impermeant tri- and tetrasaccharides to maintain the osmotic balance between the two cells. These are the first direct relative permeability determinations for a connexin-specific gap junction channel and suggest that the connexin channel with the reported highest relative permeability to anionic fluorescein dyes has a lower anion-to-cation permeability than previous estimates based on aqueous diffusion theory alone (Veenstra et al., 1995). Neyton and Trautmann (1985) used mannitol, KCl, and NaCl to determine the relative P_K, P_{Na}, and P_{Cl} (1, 0.81, 0.69) through rat lacrimal gland cell gap junction channels (connexin composition undetermined) and concluded that K^+ and Na^+ were essentially aqueous while P_{Cl} was reduced presumably by anionic charges within the pore. Our P_{Na}/P_K value of 0.78 for the rCx43 channel is in close agreement with these findings despite the

noticeable deviation of Li^+ from aqueous mobility relative to Na^+.

The γ_j of 97 pS in IPS KCl is in close agreement with other reports of the maximum γ_j of the rat or human Cx43 channel from neonatal rat cardiomyocytes or transfected SK Hep1 cells, respectively (Takens-Kwak and Jongsma, 1992; Moreno et al., 1994). The slightly higher γ_j values reported in this investigation can be attributed to the increased osmolarity of our IPSs (310 mosm, Table I). We have noticed a difference in γ_j using BAPTA-buffered IPSs relative to EGTA in all experiments on connexin-specific gap junction channels including the rCx43 channel reported here. BAPTA and EGTA could be permeable since there are reports of junctional permeability to FURA-2 in cardiac ventricular myocardium (Backx and Ter Keurs, 1993). Nonetheless, this alteration of the rCx43 maximum γ_j between EGTA- and BAPTA-buffered IPSs does not alter the cation and anion selectivity sequence results presented in this investigation since channel conductance and permeability determinations were performed using identically BAPTA-buffered IPSs.

The experiments described here provide the first evidence for an Eisenman II sequence determination of a connexin-specific channel, which implies that ionic permeability through the rCx43 channel is not limited by simple aqueous diffusion. We have previously suggested that the moderate ionic selectivities of several connexin-specific gap junction channels could be accounted for by weak anionic sites (e.g., with electrostatic potential <20 mV) (Veenstra et al., 1995). Given that the rCx43 channel exhibits the weakest ionic selectivity and highest molecular permeability to anionic fluorescent tracers of any connexin-specific channel examined to date, other more ion-selective connexin channels may exhibit selectivity sequences other than Eisenman II and display stronger ion-site interactions (greater electrostatic field potentials) than exist within the pore of the rCx43 channel.

The P_{Cl}/P_{Li} value of 0.18 is relevant to the previous estimation of the relative anion:cation permeability of connexin channels defined by the R_p coefficient (Veenstra et al., 1995). The inherent difficulty in providing a reliable estimate of relative anion:cation permeabilities using the R_p estimate methodology comes from the assumption that the permeabilities to all cations or anions are in direct proportion to the aqueous mobilities of the ions and the fact that the mobility of glutamate was an estimate based on its relative molecular weight to other molecules with known aqueous mobilities (Veenstra et al., 1995). The R_p value simply depicts the scaling factor applied to the aqueous diffusion coefficients (in place of the permeability terms in the GHK current equation) for chloride and glutamate required to achieve the experimental current (conductance) ratio observed during symmetrical equimolar Kglutamate for Kchloride substitution (Veenstra et al., 1995). This is also true of the Levitt approximation for D_x/D_o since all ionic mobilities were scaled by an assumed uniform pore radius. It is known from several types of ion channels that the highest selectivity is usually associated with a site exhibiting the narrowest restriction in pore diameter and nearby ion-site interactions (e.g., carboxyl residues for cation binding). It was also determined that if the glutamate permeability were zero, the R_p estimate for the rCx43 channel would drop to <1. The initial rCx43 channel R_p value of 1.17 drops to 0.54 if glutamate is assumed to be impermeable. Our estimate of the relative anion:cation permeability ratio of 0.71 obtained from the Levitt approximations falls within this range, suggesting that glutamate has a finite mobility in the rCx43 channel. From diffusion potential measurements, we estimate the aqueous glutamate mobility to be 50% lower than our initial estimated value of 0.345 (= 0.7/2.03 = relative aqueous mobility, μ, ($\cdot$ RT/F) = D). From the diffusion potential difference between IPS KCl and Kglutamate, we calculate an experimentally measured aqueous glutamate/chloride ratio of 0.18, which gives an aqueous diffusion coefficient of 0.365 (= 0.18 $\times$ 2.03). This is roughly half of the estimated value used in our previous calculations of the R_p value for five connexin channels. Even if the R_p estimates are adjusted accordingly, they do not approach the Cl^-/K^+ permeability ratio of 0.13 obtained from reversal potential measurements on the rCx43 channel. These shortcomings are likely due to the assumptions of an aqueous pore and ionic independence inherent to the R_p estimations.

Multi-ion occupancy is expected since the gap junction channel is a long pore, but direct cation-anion interactions are not expected for a large diameter aqueous pore. All previous permeability studies and descriptions of the generic gap junction channel have portrayed this channel as a relatively nonselective aqueous pore (e.g., Hille, 1992). Large channel theory (LCT, Zambrowicz and Colombini, 1993) predicts concentration-dependent changes in P_{Cl}/P_K which are not predicted by the GHK equation. In LCT, ionic screening of electrostatic charge contributed by the wall of the pore permits counterion flow by creating a central aqueous cylinder devoid of electrostatic charge. Other examples of cations influencing the relative permeability of anions (or vice versa) through a pore which exhibits a finite cation (or anion) selectivity have been reported (Franciolini and Nonner, 1994). One interpretation of an anion occupied site being necessary for cation permeation was developed for the amphotericin B channel by Borisova et al. (1986). The polyene antibiotics, nystatin and amphotericin B, form symmetrical channels with a relatively large pore diameter of ≈8 Å and a modest an-

ion-to-cation selectivity. Yet, in the absence of any permeant anion, the channels appear to be impermeant to cations known to be permeant in the presence of permeant anions. They were able to test their hypothesis based on the knowledge that the polyene antibiotic channel is permeant to monovalent anions and cations but not divalent anions and cations. They were able to quantitatively describe their findings by assuming that the cation transiently forms an ion pair with a bound anion at a central site in the channel. Although our data on the rCx43 channel does not distinguish between LCT and cation-dependent anion permeability theories, the estimated pore diameter of 12–14 Å is closer to the 8 Å diameter of the polyene antibiotic channel than the 30 Å diameter of the VDAC channel. A single K^+ bound to a site within the rCx43 pore reduces the effective pore diameter by 25%. This already reduces the maximum distance between a passing Cl^- and the K^+ or the wall of the pore to ≈3 Å on either side. Hence, any two ions passing each other within the rCx43 pore will at most share one water molecule and have only one additional water molecule separating them from the wall of the pore. The similarities between the conductance and permeability sequences for the monovalent cations in the rCx43 channel is not indicative of a high affinity cation binding site within the rCx43 pore, although there is evidence for a moderate selectivity for cations over anions ($P_{Cl}/P_K = 0.13$ and Eisenman series II cation selectivity sequence). Whether anion conductance in the rCx43 channel depends upon the presence of a permeant cation is a testable hypothesis which merits investigation and is a direct result of performing relative permeability measurements for the test cations and anions under asymmetric salt conditions. What has emerged from the present investigation is that electrostatic ion-site and potential ion-ion interactions are more important in gap junction channel permeability than previously appreciated. Future permeability studies should be designed to distinguish between specific models for ion permeation developed for other ion channels (Borisova et al., 1986; Zambrowicz and Colombini, 1993; Franciolini and Nonner, 1994).

This comparison illustrates the need to perform ion selectivity sequences and reversal potential experiments in order to accurately predict the relative ionic permeabilities, ion-ion and/or ion-site interactions, and dimensions of the connexin pore. Further determination of these proposed interactions will require concentration-dependent and mole-fraction relative permeability studies of the principal cations and anions used in this investigation. Analogous experiments to those performed by Borisova et al. (1986) could be more difficult here since impermeant cations and anions have not yet been identified for connexin channels. Determination of monovalent cation and anion K_ds will also provide valuable insights into the relative binding affinities of proposed binding sites within the rCx43 channel revealed by this investigation.

The relative anion:cation permeability estimate (relative Cl^-/K^+ permeability = 0.13) provided here for the rCx43 channel is 4 to 5 times lower than previous estimates of 0.52–0.69 for the relative Cl^-/K^+ permeability of rat lacrimal and earthworm median giant axon gap junction channels of unspecified connexin composition (Neyton and Trautmann, 1985; Brink and Fan, 1989). The present determinations have been made using slightly hyperosmotic solutions (310 mosm, ≈10% hyperosmotic) and therefore closely reflect physiological conditions. It seems unlikely that the connexin channel is approaching saturation under these ionic conditions and changes in connexin channel conductance associated with modification of the principal ionic salt in previous experiments have demonstrated that the channel conductance increases in equal proportion to the osmolarity change within the 270–320 mosm range (Veenstra et al., 1995).

This apparent selectivity implies that connexin channels have a diminishing permeability to organic anions of increasing size, also consistent with fluorescent tracer studies of junctional permeability (Flagg-Newton et al., 1979; Brink and Dewey, 1980). This obviously bears on the ability of anionic second messengers such as cAMP and 1,3-inositoltrisphosphate to pass through connexin-specific gap junction channels. Using anionic fluorescein derivatives, 2,7-dichlorofluorescein and 6-carboxyfluorescein, we demonstrated that rCx43 gap junctions have the highest incidence of dye transfer (100% for both dyes) and the lowest ionic selectivity of the five connexins examined thus far (chicken Cx45 and Cx43, rat Cx43, human Cx37, and rat Cx40; Veenstra et al., 1995). The present results are consistent with these previous observations, but indicate that the anionic permeability of the rCx43 channel is lower than previously thought and that the fluxes for organic anions with molecular weights of >100–400 D are significantly lower than the ionic fluxes carried by the rCx43 channel. Based on our previous ionic selectivity and dye transfer results, even lower anionic fluxes are expected for the other four connexin-specific gap junction channels.

The permeability of several fluorescent probes measured in various mammalian cell lines, many of which likely contain Cx43, demonstrated a molecular weight limit of ≈900 daltons and led to predictions of the limiting pore diameter ranging from 16 to 20 Å for mammalian gap junction channels (Flagg-Newton et al., 1979; Schwarzmann et al., 1981). The channel conductance-mobility plot for the test cations and anions in the present investigation were used to provide an estimate of the pore size based on the expected reduction in ionic mobility due to the relative radii of the ion to

the pore of the channel (Figs. 3 and 5). This provides an estimate of 12.2 Å which we initially interpreted as the estimated radius for the rCx43 channel pore. Estimates of pore size have traditionally been inferred from direct comparison of the relative permeabilities of numerous permeant ions and estimation of their effective radius or diameter relative to the pore radius or diameter. We have utilized two methods to approximate the pore size of the rCx43 channel which utilize the same frictional drag coefficient derived from hydrodynamic theory of spheres falling through an aqueous cylinder of constant diameter. The Levitt (1991) theory assumes the diffusion coefficient of the ion in the channel (D_x) relative to the bulk solution (D_o) to be reduced by an amount equal to the frictional drag coefficient taken from the hydrodynamic equation ($[1 - 2.105\alpha + 2.0865\alpha^3 - 1.7068\alpha^5 + 0.72603\alpha^6]/[1 - 0.75857\alpha^5]$). We arbitrarily chose to use the estimated radius for the pore which approximated the experimentally measured conductance of the rCx43 channel in IPS KCl based on the sum of the y-intercepts of the cation and anion conductance-mobility plots. This yielded a value of 12.2 Å. The Levitt continuum theory, as applied here, assumes a constant ionic mobility and pore diameter throughout the length of the channel. Hence, this estimate of pore size should be regarded as an upper limit for the pore radius.

Since the D_x/D_o factor for each ion was determined using its radius rather than its diameter, we initially interpreted our results of the Levitt approximation as an estimate of pore radius, although it is not entirely clear what it means to use the Levitt approximation to determine pore size from ionic conductance-mobility plots. Levitt had specific structural, electrostatic, and conductance information about the pore when he integrated the conductance profile for the nicotinic acetylcholine receptor channel. Hence, he did not have to rely on the sum of the estimated ionic conductances for his estimate of pore size. Conversely, the pore size was used to infer the conductance properties at different sites within the pore. Levitt found that the channel conductance decreased with increasing length of a narrow electrostatic region, which also predominantly determined the conductance and permeability properties of the channel (i.e., the selectivity filter affects the kinetics of ion transport as well as permeability). In our treatment of the Levitt restricted diffusion theory, we have not accounted for any specific ion-site interactions or narrowing restrictions within the pore. Our estimate of 12.2 Å for a rCx43 pore radius assumes a homogeneous pore devoid of narrow electrostatic regions which can profoundly alter the channel conductance and permeability properties. Hence, the estimate of pore size may not accurately reflect the true radius of the pore if inhomogeneities exist in the pore cross-sectional area and electrostatic potentials especially at narrower sites within the pore. We interpret our findings that the monovalent cation and anion conductance-mobility plots for the rCx43 channel are both linear and decreasing as evidence that the ion-site interactions are weak (low dehydration energy) and that the radius of the permeant ion does not approach the limiting radius of the pore. The output of the Levitt D_x/D_o equation is approximately linear for ions with ion/pore ratios of ≤ 0.40 and scaling of the aqueous mobilities for ions whose relative radii vary only by a factor of 0.1 does not deviate significantly from linearity. It should be noted that this methodology could not be applied to the rCx40 channel since the conductance-mobility plots deviated from linearity and in opposite directions (Beblo and Veenstra, 1997).

The hydrodynamic equation traditionally used to provide estimates of pore radius from relative ion permeabilities also includes a volume displacement term ($C \cdot [1 - \alpha]^2$) which takes into account the amount of water which must be displaced from the mouth of the pore for an ion to enter the cylinder. This approach yielded an estimated pore radius of 6.3 ± 0.4 Å. Relative permeability estimates have been directly correlated with spatial changes in the cross-sectional area of the selectivity filter as determined by space-filling models of amino acid side chain substitutions into the central hydroxyl ring of the nicotinic acetylcholine receptor channel (Villaroel and Sakmann, 1992). This suggests that the hydrodynamic equation and the relative permeability values of the channel in question provide a more direct interpretation of the limiting dimensions of a channel's selectivity filter. A pore radius of 6.3 ± 0.4 Å, or pore diameter of 12.6 Å, is consistent with the interpretation of the LiCl-sugar experiments since raffinose and stachyose yielded identical reversal potentials of −16.3 mV in the presence of a 115/30 mM LiCl gradient. The estimated radius of raffinose is 5.6 Å and the approximate radius of stachyose must be ≥6.4 Å which places both of these sugars near or slightly greater than the size limitation of the rCx43 pore. The conclusion that raffinose and stachyose are not permeable through the rCx43 pore is substantiated by the observation that similar ($n = 4$) experiments using mannitol failed to produce a measurable reversal potential (<1 mV, data not shown). Mannitol also dramatically reduced the channel conductance to 50 pS whereas raffinose and stachyose did not, again consistent with the interpretation that mannitol was permeable through the rCx43 pore and was unable to sustain an ionic gradient over the course of an experiment (20 min). If mannitol is permeable, its presence in the channel would displace current carrying ions from the pore, thus reducing the channel conductance. It also follows that if the chemical potential for mannitol is diminishing due to its net

diffusion through the pore, the electrochemical gradients for LiCl will also diminish in order to maintain osmotic balance. Hence, we conclude that the diameter of the rCx43 channel is ≈12 Å. This estimated diameter for the rCx43 channel is also in close agreement with the predicted maximum pore diameter of 14 Å based on the morphological model of a gap junction channel, even though the x-ray crystallography data which the model is based upon was obtained from liver gap junctional membrane plaques which are known to contain Cx32 and Cx26 instead of Cx43 (Makowski, 1984; Paul, 1986; Zhang and Nicholson, 1989). The ultimate demonstration of this awaits the determination of the largest permeant and smallest impermeant cation through the rCx43 pore. Unfortunately, TBA^+ produced noisy and short-lived channel recordings due to gradual GΩ seal breakdown over a period of <5 min which we assumed was due to the detergent action of 115 mM intracellular TBA^+ on the cell membrane. Experiments with other more hydrophilic cations are presently underway.

Based on the present findings, we predict that the rCx43 channel will have a small, finite fixed anionic electrostatic field associated with the pore and a limiting diameter of ≈12 Å. There remains a paucity of permselectivity data on connexin channels which is necessary to assist future investigations into which connexin amino acid residues contribute to the pore-forming region and how the modest "selectivity filter" of these channels is constituted. It will be interesting as efforts to determine the structure-function relationships of the connexin channels proceeds to see what models for the connexin channel pores are developed and if these predictions of channel diameter based on pore permeability properties are reasonably accurate.

The rat Cx43 transfected N2A cells were courteously provided by Dr. Eric C. Beyer, Washington University School of Medicine, St. Louis, MO 63110. The N2A cell cultures were maintained in Dr. Veenstra's laboratory by Mr. Mark G. Chilton. We wish to thank Dr. Peter R. Brink, Dept. of Physiology and Biophysics, SUNY Health Science Center, Stony Brook, NY 11794 for helpful discussions about the biophysical determinants of ionic permeability within a pore and Dr. Joseph D. Robinson for his helpful comments on the manuscript.

The research reported in this manuscript was provided by National Institute of Health grants HL-42220 to R.D. Veenstra and HL-45466 to E.C. Beyer and R.D. Veenstra. Dr. Richard D. Veenstra is currently an Established Investigator of the American Heart Association.

Original version received 23 June 1995 and accepted version received 7 January 1997.

REFERENCES

Bachx, P.H., and H.E.D.J. Ter Keurs. 1993. Fluorescent properties of rat cardiac trabeculae microinjected with fura-2 salt. *Am. J. Physiol.* 264:H1098–H1110.

Beblo, D.A., and R.D. Veenstra. 1997. Monovalent cation permeation through the connexin40 gap junction channel Cs, Rb, K, Na, Li, TEA, TMA, TBA and effects of anions Br, Cl, F, acetate, aspartate, glutamate, and NO_3. *J. Gen. Physiol.* 109:509–522.

Beyer, E.C., D.L. Paul, and D.A. Goodenough. 1990. Connexin family of gap junction proteins. *J. Membr. Biol.* 116:187–194.

Borisova, M.P., R.A. Brutyan, and L.N. Ermishkin. 1986. Mechanism of anion-cation selectivity of amphotericin B channels. *J. Membr. Biol.* 90:13–20.

Brink, P.R. 1991. Gap junction channels and cell-to-cell messengers in myocardium. *J. Cardiovasc. Electrophysiol.* 2:360–366.

Brink, P.R., and M.M. Dewey. 1980. Evidence for fixed charge in the nexus. *Nature (Lond.).* 285:101–102.

Brink, P.R., and S.-F. Fan. 1989. Patch clamp recordings from membranes which contain gap junction channels. *Biophys. J.* 56:579–593.

Dwyer, T.M., D.J. Adams, and B. Hille. 1980. The permeability of the endplate channel to organic cations in frog muscle. *J. Gen. Physiol.* 75:469–492.

Eisenman, G., and R. Horn. 1983. Ionic selectivity revisited: the role of kinetic and equilibrium processed in ion permeation through channels. *J. Membr. Biol.* 76:197–225.

Fenwick, E.M., A. Marty, and E. Neher. 1982. Sodium and calcium channels in bovine chromaffin cells. *J. Physiol. (Lond.).* 331: 599–635.

Fishman, G.I., A.P. Moreno, D.C. Spray, and L.A. Leinwand. 1991. Functional analysis of human cardiac gap junction channel mutants. *Proc. Natl. Acad. Sci. USA.* 88:3525–3529.

Fishman, G.I., D.C. Spray, and L.A. Leinwand. 1990. Molecular characterization and functional expression of the human cardiac gap junction channel. *J. Cell Biol.* 111:589–598.

Flagg-Newton, J., I. Simpson, and W.R. Loewenstein. 1979. Permeability of the cell-to-cell membrane channels in mammalian cell junction. *Science (Wash. DC).* 205:404–407.

Franciolini, F., and W. Nonner. 1994. A multi-ion permeation mechanism in neuronal background chloride channels. *J. Gen. Physiol.* 104:725–746.

Hess, P., J.B. Lansman, and R.W. Tsien. 1986. Calcium channel selectivity for divalent and monovalent cations. Voltage and concentration dependence of single channel current in ventricular heart cells. *J. Gen. Physiol.* 88:293–319.

Hille, B. 1975. Ionic selectivity of Na and K channels of nerve membranes. *In* Membranes: A Series of Advances, Vol. 3, Dynamic Properties of Lipid Bilayers and Biological Membranes. G. Eisenman, editor, Marcel Dekker, Inc., New York. 255–323.

Hille, B. 1992. Ionic Channels of Excitable Membranes. Sinaver Associates, Inc., Sunderland, MA.

Levitt, D.G. 1991. General continuum theory for multiion channel. II. Application to acetylcholine channel. *Biophys. J.* 59:278–288.

Makowski, L., D.L.D. Caspar, W.C. Phillips, and D.A. Goodenough. 1984. Gap junction structures. V. Structural chemistry inferred from X-ray diffraction measurements on sucrose accessibility and trypsin susceptibility. *J. Mol. Biol.* 174:449–481.

Manivannan, K., S.V. Ramanan, R.T. Mathias, and P.R. Brink. 1992. Multichannel recordings from membranes which contain gap junctions. *Biophys. J.* 61:216–227.

Moreno, A.P., J.C. Saez, G.I. Fishman, and D.C. Spray. 1994. Human connexin43 gap junction channels: regulation of unitary conductances by phosphorylation. *Circ. Res.* 74:1050–1057.

Neyton, J., and A. Trautmann. 1985. Single channel currents of an intercellular junction. *Nature (Lond.).* 317:331–335.

Nightingale, E.R. 1959. Phenomenological theory of ion solvation. Effective radii of hydrated ions. *J. Phys. Chem.* 63:1381–1387.

Paul, D.L. 1986. Molecular cloning of cDNA for rat liver gap junction protein. *J. Cell Biol.* 103:123–134.

Ramanan, S.V., and P.R. Brink. 1993. Multichannel recordings from membranes which contain gap junctions. II. Substates and conductance shifts. *Biophys. J.* 65:1387–1395.

Reed, K.E., E.M. Westphale, D.M. Larson, H.-Z. Wang, R.D. Veenstra, and E.C. Beyer. 1993. Molecular cloning and functional expression of human connexin37, an endothelial cell gap junction protein. *J. Clin. Invest.* 91:997–1004.

Rup, D.M., R.D. Veenstra, H.-Z. Wang, P.R. Brink, and E.C. Beyer. 1993. Chick connexin-56, a novel lens gap junction protein. *J. Biol. Chem.* 268:706–712.

Schwarzmann, G., H. Wiegandt, B. Rose, A. Zimmerman, D. Ben-Haim, and W.R. Loewenstein. 1981. Diameter of the cell-to-cell junctional membrane channels as probed with neutral molecules. *Science (Wash. DC).* 213:551–553.

Swenson, K.I., J.R. Jordan, E.C. Beyer, and D.L. Paul. 1989. Formation of gap junctions by expression of connexins in *Xenopus* oocyte pairs. *Cell.* 57:145–155.

Takens-Kwak, B.R., and H.J. Jongsma. 1992. Cardiac gap junctions: three distinct single channel conductances and their modulation by phosphorylating treatments. *Pflüg. Arch.* 422:198–200.

Veenstra, R.D. 1991. Physiological modulation of cardiac gap junction channels. *J. Cardiovasc. Electrophysiol.* 2:168–189.

Veenstra, R.D., and P.R. Brink. 1992. Patch clamp analysis of gap junctional currents. *In* Cell-Cell Interactions: A Practical Approach. B. Stevenson, D.L. Paul, and W. Gallin, editors. IRL Press. Oxford. 167–201.

Veenstra, R.D., H.-Z. Wang, E.M. Westphale, and E.C. Beyer. 1992. Multiple connexins confer distinct regulatory and conductance properties of gap junctions in developing heart. *Circ. Res.* 71: 1277–1283.

Veenstra, R.D., H.-Z. Wang, E.C. Beyer, and P.R. Brink. 1994*a*. Selective dye and ionic permeability of gap junction channels formed by connexin45. *Circ. Res.* 75:483–490.

Veenstra, R.D., H.-Z. Wang, E.C. Beyer, S.V. Ramanan, and P.R. Brink. 1994*b*. Connexin37 forms high conductance gap junction channels with subconductance state activity and selective dye and ionic permeabilities. *Biophys. J.* 66:1915–1928.

Veenstra, R.D., H.-Z. Wang, D.A. Beblo, M.G. Chilton, A.L. Harris, E.C. Beyer, and P.R. Brink. 1995. Selectivity of connexin-specific gap junctions does not correlate with channel conductance. *Circ. Res.* 77:1156–1165.

Villarroel, A., and B. Sakmann. 1992. Threonine in the selectivity filter of the acetylcholine receptor channel. *Biophys. J.* 62:196–208.

Werner, R., E. Levine, C. Rabadan-Diehl, and G. Dahl. 1989. Formation of hybrid cell-cell channels. *Proc. Natl. Acad. Sci. USA.* 86: 5380–5384.

Zambrowicz, E.B., and M. Colombini. 1993. Zero-current potentials in a large membrane channel: a simple theory accounts for complex behavior. *Biophys. J.* 65:1093–1100.

Zhang, J.-T., and B.J. Nicholson. 1989. Sequence and tissue distribution of a second protein of hepatic gap junctions, Cx26, as deduced from its cDNA. *J. Cell Biol.* 109:3391–3401.